International Journal of Biological Macromolecules 283 (2024) 137906

Contents lists available at ScienceDirect

International Journal of Biological Macromolecules

journal homepage: www.elsevier.com/locate/ijbiomac

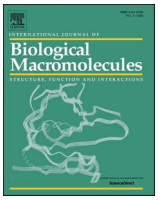

Tailoring the morphology and antibacterial activity of PBAT and thermoplastic cassava starch blown films with phosphate derivatives

Phanwipa Wongphan [a], Cristina Nerín [b], Nathdanai Harnkarnsujarit [a,c,*]

[a] Department of Packaging and Materials Technology, Faculty of Agro-Industry, Kasetsart University, 50 Ngam Wong Wan Rd., Latyao, Chatuchak, Bangkok 10900, Thailand
[b] Department of Analytical Chemistry, Aragon Institute of Engineering Research I3A, EINA-University of Zaragoza, Maria de Luna 3, 50018 Zaragoza, Spain
[c] Center for Advanced Studies for Agriculture and Food, Kasetsart University, 50 Ngam Wong Wan Rd., Latyao, Chatuchak, Bangkok 10900, Thailand

ARTICLE INFO

Keywords:
Cassava starch
Polybutylene adipate terephthalate
Phosphate compound
Biodegradable
Blown film extrusion
Packaging

ABSTRACT

Phosphate derivatives contain a high number of reactive groups that interact functionally with various polymers. Tetrasodium pyrophosphate ($Na_4P_2O_7$), sodium tripolyphosphate ($Na_5P_3O_{10}$), and sodium hexametaphosphate ($(NaPO_3)_6$) were incorporated into bioplastic polybutylene-adipate-terephthalate (PBAT) blended with thermoplastic cassava starch (TPS) in blown films. Their physicochemical, morphological, thermal, and antimicrobial properties were investigated. PBAT/TPS blended films were compounded via blown film extrusion to produce functional packaging. Infrared spectra indicated starch modification through the disruption of anhydroglucose monomer units, analyzed by ATR-FTIR, providing a more amorphous fraction and altering the properties of the films. PBAT/TPS films containing phosphate compounds exhibited non-homogeneous structures, with dispersed clumps within the film matrices that decreased tensile strength. The incorporation of phosphate compounds modified the storage modulus and relaxation temperature of PBAT/TPS films, influencing molecular mobility, decreasing heat transfer efficiency in seal strength, and enhancing stiffness due to starch disruption and interaction between the phosphate compound and the PBAT/TPS matrix. Wettability and permeability of PBAT/TPS films were modified by changes in polymer structure.

1. Introduction

Environmentally friendly packaging materials minimize non-biodegradable plastic waste generation, thereby adhering to the sustainable development goals (SDGs) as a global policy. Commonly used economic biodegradable plastics are hydrophobic polyesters, namely polybutylene adipate terephthalate (PBAT), polybutylene succinate (PBS) and polycaprolactone (PCL). PBAT is rarely used in the commercial market due to its high cost and limited material performance compared with petroleum-based materials [1–3]. PBAT is a biodegradable aromatic-aliphatic copolyester with good processing stability and excellent biodegradation properties but is rarely used alone due to their high manufacturing cost and low mechanical properties, compared to other bioplastics. Additionally, its inferior properties often times limit the production scale-up [2,3]. To address these limitations, blending PBAT with other bioplastics, such as thermoplastic starch (TPS), has been explored. TPS, derived from starch, offers advantages like availability, low cost, and non-toxicity. However, its poor processability, mechanical properties, and low thermal stability limit its standalone use. Blending PBAT with TPS can improve the cost-effectiveness of PBAT and enhance the processability and stability of starch. However, the interfacial adhesion between the two polymers is crucial for optimal performance. Copious research has improved performance and reduced cost by blending bioplastics with materials having high mechanical and barrier properties [3–6]. Therefore, PBAT/TPS blend is filled with additives to enhance and improve the properties of the blended film to have better properties [1,4,7,8].

Starch modification by covalent linking strongly enhances interfacial adhesion, improves hydrophobicity and enhances TPS granule disruption in hydrophobic materials [2,3,5,9]. Starch can be modified by chemical and physical procedures through esterification and phosphorylation processes [10,11]. Wei et al. [12] suggested that starch phosphorylation generated intra and intermolecular bonds through crosslinking of phosphate groups, leading to starch unit disruption and

* Corresponding author at: Department of Packaging and Materials Technology, Faculty of Agro-Industry, Kasetsart University, 50 Ngam Wong Wan Rd., Latyao, Chatuchak, Bangkok 10900, Thailand.
E-mail addresses: phanwipa.w@ku.th (P. Wongphan), cnerin@unizar.es (C. Nerín), nathdanai.h@ku.ac.th (N. Harnkarnsujarit).

https://doi.org/10.1016/j.ijbiomac.2024.137906
Received 3 May 2024; Received in revised form 9 November 2024; Accepted 19 November 2024
Available online 20 November 2024

the formation of mono-starch and di-starch phosphates. Phosphate compounds commonly used as crosslinking agents include sodium tripolyphosphate, sodium trimetaphosphate and phosphoryl chloride [10,12]. Phosphate derivatives such as tetrasodium pyrophosphate ($Na_4P_2O_7$), sodium tripolyphosphate ($Na_5P_3O_{10}$) and sodium hexametaphosphate ($Na_6(PO_3)_6$) are widely used to improve food packaging functional performance [13,14]. The starch is modified by grafting or modification at hydroxyl groups onto the starch backbone that are then available for covalent bonding and enhance the hydrophobic phase for interaction with PBAT, while also improving interfacial transesterification, depending on the substance modification [13,15]. In addition, adding additive compounds to polymers such as sodium nitrite, sodium erythorbate, nisin, and titanium dioxide can enhance the efficiency and performance of packaging. Furthermore, the addition of substances may also enhance the functionality of food packaging, such as increasing shelf life, as the additives commonly used in the food industry act as preservatives [2,3,9].

This research investigates the impact of incorporating phosphate derivatives with different chain structures and phosphate group numbers namely $Na_4P_2O_7$ has a short chain structure, consisting of two phosphate units linked together, $Na_5P_3O_{10}$ has a longer chain structure, consisting of three phosphate units linked together, and $Na_6(PO_3)_6$ has a ring structure, consisting of six phosphate units linked together in a hexagonal pattern on the properties of TPS/PBAT bioplastic films. By addressing the limitations of high PBAT cost and poor TPS formability, we aim to enhance the films' barrier properties, mechanical strength, thermal resistance, and antimicrobial activity. A key strength of this study is its innovative approach of using industrial-scale blown film extrusion to produce functional bioplastic films. This method offers significant advantages over traditional solvent casting techniques, making it more suitable for commercial applications. By utilizing various characterization techniques (FTIR, NMR, etc.). Aim to gain a deeper understanding of the structure-property relationships of the modified films. The findings of this research will contribute to the commercialization of PBAT/TPS blown film blends and promote the development of sustainable packaging solutions.

2. Materials and methods

2.1. Materials

Native cassava starch was purchased from Siam Modified Starch Co., Ltd., Thailand. PBAT (Ecoflex®F Blend C1200) was supplied by Fresh Bag Co., Ltd., Thailand. The glycerol used was a commercial grade product from Patum Vegetable Oil Co., Ltd., Thailand. Phosphate derivative compounds as food grade products including tetrasodium pyrophosphate ($Na_4P_2O_7$, phosphate 53.6 %), sodium tripolyphosphate ($Na_5P_3O_{10}$, phosphate 57.8 %) and sodium hexametaphosphate ($Na_6(PO_3)_6$, phosphate 68.2 %) were purchased from Thai Food and Chemical Co., Ltd., Thailand.

2.2. Preparation of PBAT/TPS pellets by extrusion

Phosphate derivatives namely $Na_5P_3O_{10}$, $Na_6(PO_3)_6$ and $Na_4P_2O_7$ at 0, 1, 3 and 5 % (%*w*/w of film concentration) were dissolved in 35 % (*w*/w) glycerol using a magnetic stirrer (C-MAG HS, IKA Co., Germany) until complete dissolution (1–2 h at 90 °C). Each slurry was mixed with dried starch powder (kept in a hot-air oven at 50 °C for 18 h) using a dough mixer (SC-236A, Stelang, China) for 10 min. The mixtures were transformed into TPS pellets with and without phosphate compounds using a twin-screw extruder with L/D ratio of 40 and screw diameter 20 mm (Labtech Engineering, Samut Prakan, Thailand). The temperature profile from the barrel to the die was 90/95/110/120/125/135/140/140/145/145 °C with screw speed 180 rpm. The average operation time was 45 min/kg. The extrudate TPS was cut into 2.5 mm pellets. The sample without the phosphate derivatives was used for the control sample as TPS at 0 % of phosphate derivative. The sample with phosphate compound means TPS containing phosphate compound at 1,3 and 5 % phosphate compound.

The PBAT and extrudate TPS pellets were blended at ratio 50PBAT/50TPS (PBAT/TPS) using a twin-screw extruder. A 50/50 ratio of PBAT and TPS was used in a ratio of 50/50 to provide continuity in equal proportions of the polymer phase. The temperature profile was 95/100/110/120/130/135/140/145/150/150 °C with screw speed and feeding screw speed 220 and 20–25 rpm, respectively. The average operation time was 30 min/kg. The blend was cut into 2.5 mm pellets and kept in Ziploc bags.

2.3. Preparation of blown-film extrusion from PBAT/TPS pellets

The PBAT/TPS blended pellets were dried in a hot-air oven at 50 °C for 18 h. PBAT/TPS with and without phosphate compound films using a single-screw blown film extruder with L/D ratio of 30 and screw diameter 25 mm (Labtech Engineering, Samut Prakan, Thailand). The temperature profile from the hopper to the ring-shaped die was 140/145/145/150/150/145/145 °C with screw speed 28–34 rpm and nip roll speed 2.2–2.5 rpm. The film thickness was approximately 0.04 mm. The blown films were stored in aluminum bags at room temperature before testing. The code of samples namely PBAT/TPS as a control film which no contained phosphate compound (0 %) and PBAT/TPS containing each phosphate 1, 3 and 5 % which showed the percentage of phosphate.

2.4. Characterization of PBAT/TPS films

2.4.1. Fourier transform infrared analysis (FTIR)

The characteristic chemical functional groups were identified using a Bruker Tensor 27 FTIR Spectrometer (Bruker OPTIK GmbH, Germany). Triplicate spectra were analyzed using the spectrum software OPUS 6.5. All samples were previously kept in silica gel for 48 h to reduce moisture and humidity. The infrared absorption spectra of the film samples were recorded at room temperature (25 ± 1 °C) between 500 and 4000 cm^{-1} at a resolution of 4 cm^{-1} (co-added 64 scans) with the attenuated total reflectance (ATR) mode which the intensity of FTIR peak is independent of the thickness. The spectra were standardized with the spectrum of air.

The intensity ratios between absorption peaks at 1711 and 1730 (I 1711/1730) and 3325 and 729 cm^{-1} (I 3325/729) attributed to the degree of crystallinity in PBAT and hydrogen bonding of PBAT/TPS blown films, respectively. FTIR and the intensity ratios of the absorption peaks were averaged from three measurements.

2.4.2. Proton nuclear magnetic resonance (^1H NMR)

The ^1H NMR spectra were recorded using an Ascend TM 600/Advance III HD (Bruker, Switzerland). The solvents for dissolution of PBAT/TPS films with and without phosphate compounds (10 mg) were $CDCl_3$ and one drop of DMSO-d_6 to enhance TPS dissolution. Chemical shifts were recorded in parts per million (ppm) using tetramethylsilane as the standard and operated at 600 MHz.

2.4.3. X-ray diffraction (XRD)

XRD diffractograms were determined for crystallinity using X-ray diffraction (Diffractometer D8, Bruker AXS, Germany) with Cu Kα radition ($\lambda = 0.154$ nm) operating at 30 mA and 40 kV. The samples were scanned from $2\theta = 4$ to 40° at a scan rate of 0.8 s/step with step size of 0.02°. The degree of crystallinity was calculated from the fraction of the integrated area of crystalline peaks and the total diffraction area using MDI Jade 6 software (Materials Data, Inc., USA).

2.4.4. Transparency

The PBAT/TPS films were cut into rectangular pieces and analyzed for light transmission using a UV–visible spectrometer (Evolution 300 UV–Vis Spectrophotometer, USA). Transmittance values of the three

films were measured at the ultraviolet range (wavelength 200–400 nm) and visible light range (wavelength 400–800 nm) with a speed of 600 nm/min.

2.4.5. Scanning electron microscopy with energy dispersive X-ray spectroscopy (SEM-EDX)

SEM-EDX mapping images were determined for the interface morphologies of PBAT/TPS films with and without phosphate compounds using a scanning electron microscope coupled with an energy dispersive X-ray spectroscope (SEM-EDX, FEI Quanta 450, Thermo Fisher Scientific, Massachusetts, USA) at an accelerating voltage of 10 kV. Sample cross-sections were prepared in liquid nitrogen and freeze-cracked before placing on a metal stub by conductive adhesive. The film samples were dried and gold-coated under a vacuum using a Quorum Technology Polaron Range SC7620 Sputter Coater (Quorum Technologies Ltd., UK). Morphological images were taken at magnifications of 250× and 1500× for surface and cross-section microstructures, respectively.

2.4.6. Atomic force microscopy (AFM)

Topography images of sample surfaces were determined using a 225 μm length cantilever over a region by AFM scanning (AFM, MFP-3D-Bio, Asylum Research, USA) with 190 kHz resonance frequency at a scan rate of 0.8 Hz and 8 nm nominal tip radius curvature. Figures were generated using AGgyleL software.

2.4.7. Differential scanning calorimetry (DSC)

Thermal characteristics were analyzed using a differential scanning calorimeter (DSC 1, STAR^e system, Mettler Toledo, Switzerland) with heating rate of 10 °C/min under nitrogen atmosphere at a flow rate of 25 mL/min. Temperature ranges for the two-step analysis were 50 to 250 °C and 250 to 25 °C for heating and cooling steps, respectively.

2.4.8. Thermogravimetric analysis (TGA)

Thermal stability of the samples was determined by thermogravimetric analysis (TGA 2 STAR^e System, Mettler Toledo, Switzerland). The heating temperature and heating rate were 30–900 °C and 10 °C/min, respectively under a nitrogen atmosphere at a flow rate of 20 mL/min. Results were reported as percentage of weight loss and 1st derivative weight loss to represent degradation temperature (T_d).

2.4.9. Dynamic mechanical thermal analysis

Relaxation temperatures of the samples were determined using a dynamic mechanical thermal analyzer (DMTA, Mettler Toledo-DMA 1, Switzerland). Heating temperatures and heating rates were − 100 to 100 °C and 2 °C/min, respectively at 5.0, 10.0 and 20.0 Hz. Results as the tan δ peak represented the ratio of storage to loss modulus.

2.4.10. Mechanical properties

Mechanical properties according to ASTM D882–88 as tensile strength (TS) and elongation at break (EB) were determined using an Instron Universal Testing Machine (Model 5965, Instron, USA). The samples were cut into rectangles of 150 mm length and 25.4 mm width with 0.04 mm average thickness. All samples were conditioned in a chamber at 50 ± 2 % RH for 48 h before testing. The testing was performed at a speed of 500 mm/min with distance between the gap 5 cm. Results were recorded as the average value from five specimens.

2.4.11. Seal strength

Seal strength was measured according to ASTM F88/F88M-15 using an Instron Universal Testing Machine (Model 5965, Intron, USA) at a rate of 200 mm/min. The method was modified from Bumbudsanpharoke et al. [16]. The samples were cut into rectangles (150 mm × 25.4 mm). The sealing temperature was 90 ± 5 °C with pressure and sealing time 300–350 kPa and 1 s, respectively. The results were recorded as the average value from five specimens.

2.4.12. Contact angle (CA)

Wettability of the film surfaces was determined by dropping 3 μl of distilled water on the surface with a micro-syringe using SCA 20 software (OCA 15 EC, Data Physics Instruments GmbH, Germany). All samples were conditioned in a chamber at 50 % RH at room temperature for 48 h before testing. The images and contact angle values (ten points at different places for three samples) were immediately recorded.

2.4.13. Water vapor permeability (WVP)

The standard cup method according to ASTM E96–80 was used to determine WVP. The cups were conditioned in a chamber for 48 h at 25 ± 2 °C and 50 ± 2 % RH. Each sample was placed on a metal cup filled with 25 g of dried silica gel and sealed with an O-ring using hot paraffin wax. The sealed cups were placed in a humidity chamber at 25 ± 2 °C and 50 ± 2 % RH. The WVP of each sample was obtained from the average of three specimens. The WVP values calculated from Eq. (1) involved the water vapor transmission rate (WVTP), thickness and water vapor pressure difference between each side of the films.

$$\mathrm{WVP} = \frac{(\mathrm{WVTR} \times \mathrm{Thickness})}{\text{Water vapor pressure difference}} \quad (1)$$

where WVTR was derived from the slope of the straight-line weight increase ($R^2 > 0.99$), with samples weighed until constant weight.

2.4.14. Oxygen permeability (OP)

OP was analyzed using an oxygen transmission rate analyzer (Illinois Instruments, Inc., Johnsburg IL, USA) following ASTM D3985. Triplicate OP values were calculated from Eq. (2) involving the oxygen transmission rate (OTP), thickness and partial pressure difference between each side of the films.

$$\mathrm{OP} = \frac{(\mathrm{OTR} \times \mathrm{Thickness})}{\text{Partial pressure difference}} \quad (2)$$

2.5. Antimicrobial activity of PBAT/TPS films

The antimicrobial activity of the films was determined using a combination of turbidity measurement and the *Escherichia coli* count following the modified method from Laorenza & Harnkarnsujarit [17]. The *E. coli* stain was cultured in liquid nutrient broth media (NB, HiMedia Laboratories Pvt. Ltd., India), and incubated at 37 °C for 24 h. Films (1 g) were cut into strip and were added mixed solution (1 mL of NB: 9 mL of 0.1 % peptone solution). The turbidity of the triplicate mixed solutions was then measured by incubating them at 37 °C and recording the absorbance at a wavelength of 620 nm every day for 5 days using a spectrophotometer (Genesys 10UV, Thermo Electron Corporation, USA). The 0.1 % peptone solution as a blank. Then, the *Escherichia coli* counts were determined using the mixed solutions, which were diluted to 10^{-4} and 10^{-5} and spread on nutrient agar media (NA, HiMedia Laboratories Pvt. Ltd., India). The *E. coli* colonies were counted after incubation at 37 °C for 24 h. The results were expressed as log CFU/mL.

2.6. Statistical analysis

The experimental results were generated figures using Microsoft Excel software and statistically analyzed using IBM SPSS Statistics Version 22 (IBM Inc., USA), one-way analysis of variance (ANOVA) and Duncan's test, with significant differences set at the 5 % level.

3. Results and discussion

3.1. Fourier transform infrared spectroscopy (FTIR)

A schematic illustration of the chemical reactions is shown in Fig. 1a.

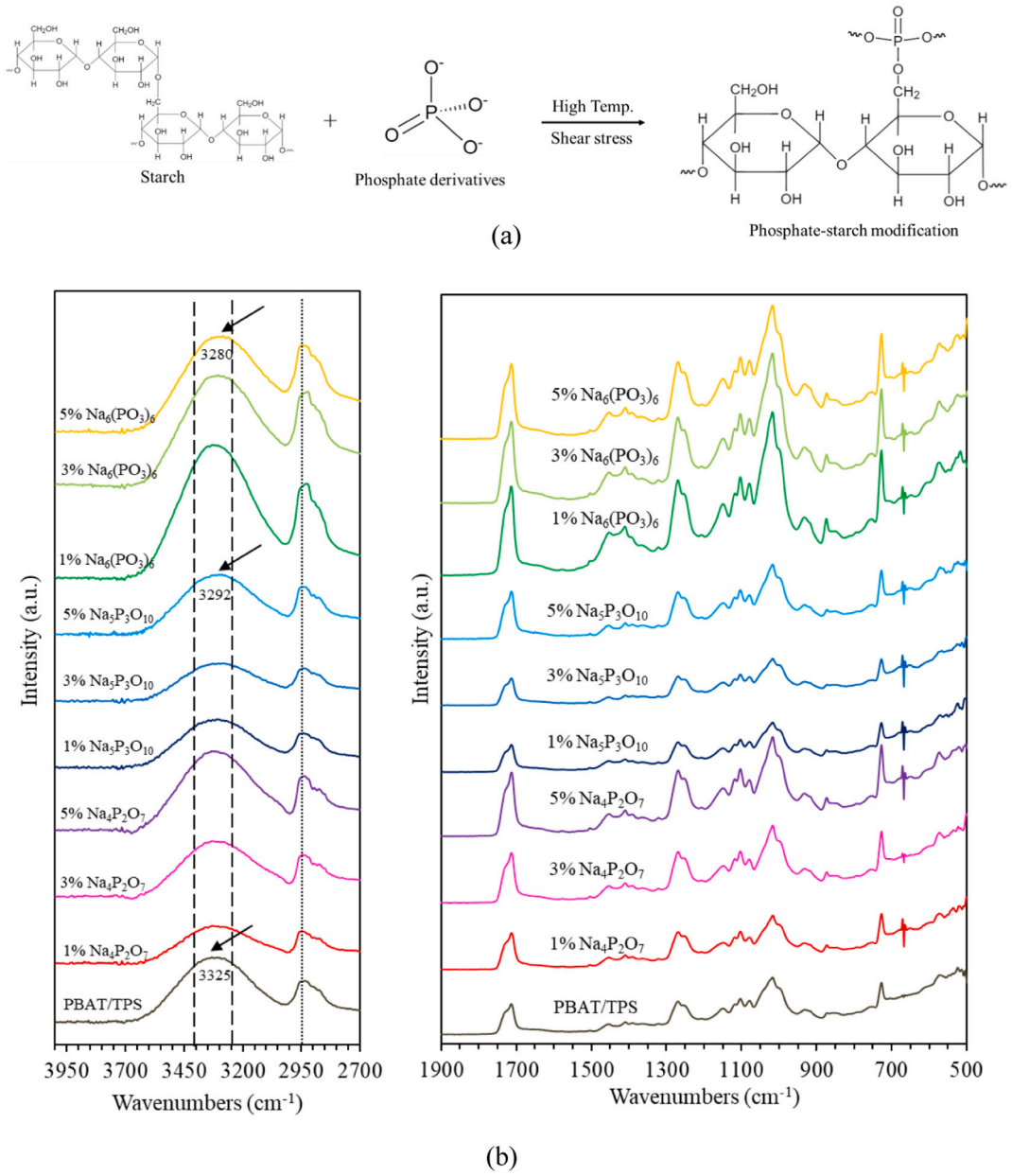

Fig. 1. (a) Schematic of the chemical reactions and chemical structures, (b) FTIR absorption spectra of blend films, (c) intensity ratios of IR peaks, and (d) ^{1}H NMR spectra of PBAT/TPS blend films containing tetrasodium pyrophosphate ($Na_4P_2O_7$), sodium tripolyphosphate ($Na_5P_3O_{10}$), and sodium hexametaphosphate ($Na_6(PO_3)_6$) at difference ratios (0, 1, 3 and 5 %).

These reactions occurred randomly with substitution of the amylopectin unit at the C-2, C-3, and C-6 positions of the anhydroglucose monomer unit, with chemical substitution more pronounced at the C-6 position [12,18]. Phosphate substitution produces mono-starch phosphate, di-starch phosphate and crosslinked starch, categorized by the reaction as esterification and combined treatments of mono- and di-starch phosphate [11,18].

The IR absorption spectra between 500 and 1500 cm^{-1} are shown in Fig. 1b as the polymer fingerprint of PBAT/TPS film containing $Na_4P_2O_7$, $Na_5P_3O_{10}$ and $Na_6(PO_3)_6$. The characteristic IR peaks of PBAT at 729 and 873 cm^{-1} were assigned to C—H out-plane bending vibration of the aromatic ring, with 1267 cm^{-1} for C—O stretching vibration of asymmetric aromatic esters and 1410 cm^{-1} for $–CH_2–$ deformation. Strong absorption between 1700 and 1750 cm^{-1} was attributed to C═O stretching vibration of the carbonyl groups [16]. The peak at 1711 cm^{-1} was attributed to the crystalline phase that merged with a shoulder at 1730 cm^{-1} attributed to the amorphous phase in PBAT. The intensity ratio between 1711 and 1730 cm^{-1} ($I_{1711/1730}$) represented the degree of crystallinity in PBAT, as shown in Fig. 1c the 1711 cm^{-1} bands relative to the 1730 cm^{-1} band indicates a higher degree of crystallinity and is more sensitive to the crystalline environment of the ester groups [8,19–22]. The incorporation of 1–5 % $Na_4P_2O_7$ and $Na_5P_3O_{10}$ significantly enhanced the ordered PBAT structure, while 1–5 % $Na_6(PO_3)_6$ had an insignificant effect on the crystallization of PBAT probably attributed to the composition of $Na_6(PO_3)_6$, which consists of the phosphate hexamer as a cyclic structure that inhibited the ordered PBAT. The results suggested that PBAT/TPS blends with $Na_4P_2O_7$ and $Na_5P_3O_{10}$ impacted the vibration of the C═O carbonyl group.

The absorption bands in the starch region showed peaks at 1047 and 1018 cm^{-1} that were ascribed to the C—O bond in C–O–C and C–O–H

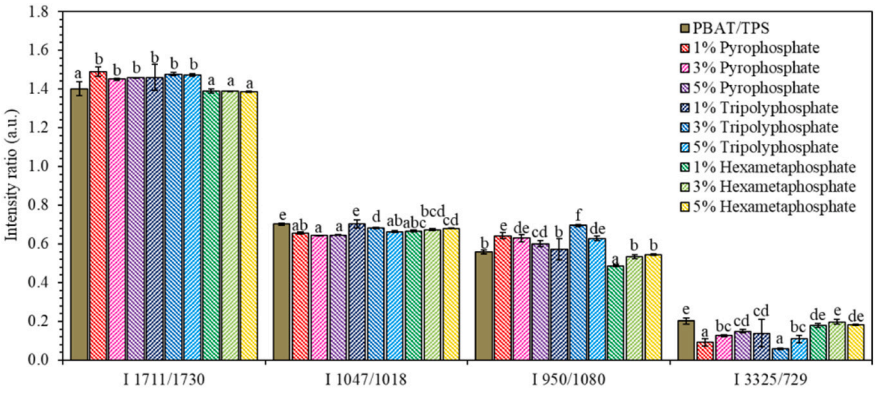

(c)

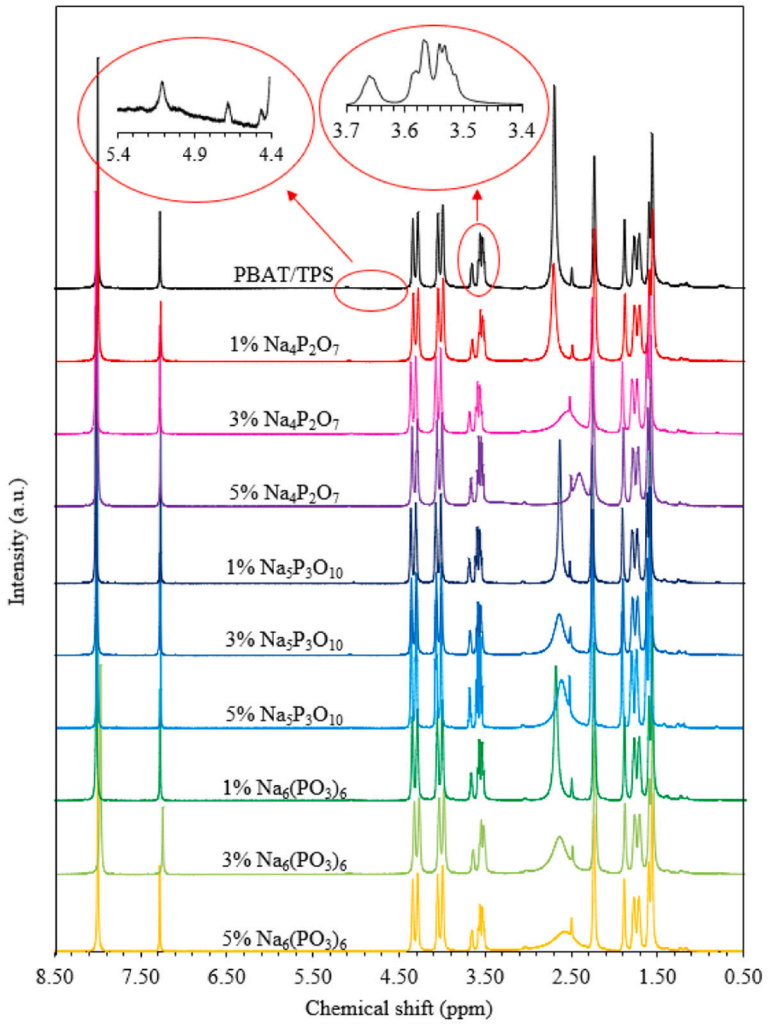

(d)

Fig. 1. (*continued*).

stretching vibration as crystalline and amorphous structures of starch, respectively [23,24]. Duckworth, Maddocks, Rahatekar & Barbour [25] investigated the IR peaks of $Na_6(PO_3)_6$, which were located at 1239, 1071 and 867 cm^{-1}, attributed to P═O, P—O and P–O–P, respectively. Film containing phosphate provided peaks at 895, 950–1090 and 1150–1400 cm^{-1}, indicating asymmetric vibration stretching of P–O–P, P–O–C and P═O stretching vibration, respectively [11,24]. The PBAT/TPS incorporated phosphate compounds showed a new peak at 665 cm^{-1} that was assigned to C–O–P vibrations, indicating starch phosphorylation. PBAT/TPS incorporated with $Na_4P_2O_7$, $Na_5P_3O_{10}$ and $Na_6(PO_3)_6$ affected starch crystallization. Increasing the concentration of phosphate compounds significantly decreased the ordered structure because the glycosidic linkages were disrupted by the phosphate groups leading to increased amorphous structures. Phosphorylation of the starch molecules gave bulky structures in the chains, preventing aggregation and an ordered structure [26].

The absorption peak located between 3012 and 3640 cm^{-1} corresponded to the hydroxyl stretching vibration of the intra and

intermolecular hydrogen bonding of the anhydroglucose unit monomer of starch and glycerol (Fig. 1b). Peaks at 2925 and 2870 cm^{-1} were attributed to antisymmetric and symmetric stretching of the C—H bonds [23,24]. The shape and intensity of the hydroxyl and C—H stretching vibration absorption peaks were modified, depending on the number and concentration of phosphate group. The hydroxyl peak of 5 % $Na_5P_3O_{10}$ and 5 % $Na_6(PO_3)_6$ shifted to lower wavenumbers from 3325 cm^{-1} to 3292 and 3280 cm^{-1}, respectively indicating increasing hydrogen bonding strength. These peaks became broader when containing 1–3 % $Na_4P_2O_7$ and 1–5 % $Na_5P_3O_{10}$ and the ratio of hydrogen bonding ($I_{3325/729}$) significantly decreased because the phosphate groups destroyed the hydrogen bonding via phosphate-starch interaction, corresponding to a decrease in the intensity of P–O–C and C–O–C ($I_{950/1080}$). The phosphate-starch modification replaced the hydroxyl group with a phosphate group, suggesting $Na_5P_3O_{10}$ had the most phosphate modification. The C—H stretching was modified and shifted to lower wavenumbers because the polymer formed the covalent bonding (P–O–C) between the anhydroglucose unit and phosphate leading to stronger interaction. The results showed that $Na_4P_2O_7$, $Na_5P_3O_{10}$ and $Na_6(PO_3)_6$ displayed interactions of a chemically modified polymeric matrix via starch phosphorylation, depending on the type and concentration of the phosphate groups.

3.2. Proton nuclear magnetic resonance (^{1}H NMR)

The ^{1}H NMR spectra exhibited chemical shift (δ) of the proton that identified the character of the chemical structure and modification. Fig. 1e shows that the chemical shift of PBAT/TPS with and without $Na_4P_2O_7$, $Na_5P_3O_{10}$ and $Na_6(PO_3)_6$ gave a chemical shift peak at 7.28 ($CDCl_3$) and 2.5 ppm (DMSO-d_6) representing the solvents for PBAT and TPS dissolution, respectively [27,28]. The PBAT/TPS (control) film provided peaks at 1.5–2.0, 4.0–4.3 and 8.0 ppm associated with the inner and outer methylene groups and the benzene ring in the PBAT structure, respectively [27]. The peak at δ = 3.3–3.7 ppm was assigned to the anhydroglucose unit, while glycerol as a plasticizer for TPS consisted of 3.5–3.6 ppm for protons at positions C3, C5 and C6 and 3.65 ppm for protons at positions C2 and C4 of the anhydroglucose unit. The TPS phase provided δ = 4.46 ppm for –OH in glycerol [1,28]. Starch consists of glycosidic linkages that exhibit protons of –OH at positions α-1,6 and α-1,4 for δ = 4.7 and 5.1 ppm, respectively [1]. PBAT/TPS film with $Na_4P_2O_7$, $Na_5P_3O_{10}$ and $Na_6(PO_3)_6$ showed that the intensity of δ = 4.7 slightly decreased, indicating that the α-1,6 glycosidic linkages were disrupted during extrusion and confirming the phosphate-starch modification (Supplement 1). The PBAT/TPS film containing $Na_4P_2O_7$, $Na_5P_3O_{10}$ and $Na_6(PO_3)_6$ showed modified chemical shift at δ = 2.7 ppm that was assigned to the methylene proton connecting the ester groups such as carbonyl and phosphate groups. These peaks changed and became broader because the electric charge of the sodium ion (Na^+) in the matrix promoted electron resonance as an intramolecular effect that was assigned to protons below or above the plane of the benzene ring, depending on the concentration of phosphate compounds used [29,30]. The results suggested that the phosphate groups modified the chemical structure in starch and PBAT phases by disrupting hydrogen bonding and proton resonances.

3.3. X-ray diffraction (XRD)

The XRD patterns of PBAT/TPS films indicated that the crystallinity was modified by the contained phosphate compounds, as displayed in Fig. 2a. The XRD pattern showed peaks at 2θ = 16.2°, 17.1°, 20.4°, 23.2° and 24.5° corresponding to the five scattering angles in PBAT, while the peaks at 2θ = 13.1°, 19.9° and 24.5° corresponded to the crystalline TPS structure [16,23]. Incorporation of phosphate modified the crystalline peaks at 2θ = 13.1° and 19.9° that became broader, while the crystalline PBAT structure at 2θ = 20.4° and 24.4° had higher peaks, indicating that phosphate influenced both crystalline structures. Incorporation of 1–5 %

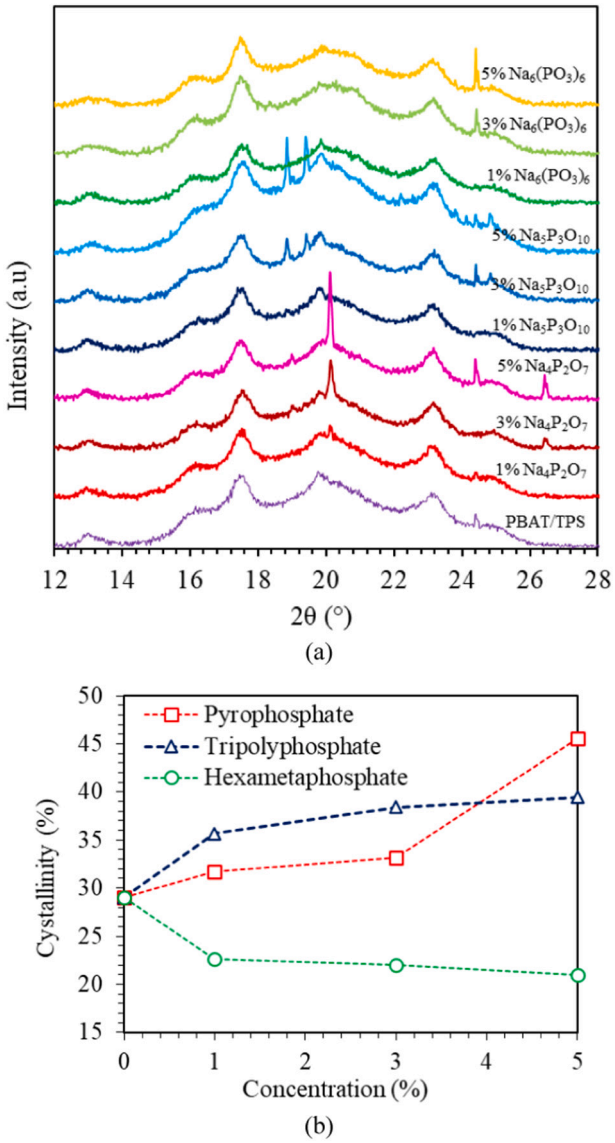

Fig. 2. (a) XRD diffractograms and (b) degree of crystallinity of PBAT/TPS blend films containing tetrasodium pyrophosphate ($Na_4P_2O_7$), sodium tripolyphosphate ($Na_5P_3O_{10}$), and sodium hexametaphosphate ($Na_6(PO_3)_6$) at different ratios (0, 1, 3 and 5 %).

$Na_4P_2O_7$ and $Na_5P_3O_{10}$ into PBAT/TPS film gave new peaks at 18.9°, 19.4° and 20.1°, exhibiting crystalline peaks of phosphate groups depending on the concentration [31]. $Na_6(PO_3)_6$ addition effectively impacted the crystallinity of TPS due to diffraction in starch. The peak at 2θ =19.9° became wider and broader, indicating that $Na_6(PO_3)_6$ improved the TPS amorphous phase and formed a crosslinked structure [31–34]. These results were consistent with those from El-Naggar et al. [31] who found that the crystalline peak disappeared at 2θ =19.2° because the crosslinked starch using phosphate compounds changed with the incorporation of hydroxyl starch in the phosphate groups. The degree of crystallinity (Fig. 2b) showed that incorporation of $Na_6(PO_3)_6$ reduced the ordered structure because of covalent bonds between the polymer chains that reduced chain mobility, while $Na_4P_2O_7$ and $Na_5P_3O_{10}$ also provided covalent bonds but the degree of crystallinity improved because both compounds reduced starch crystallinity and the PBAT ordered structure increased, related to the FTIR intensity of $I_{1711/1730}$ (Fig. 1c). The new crystallization peaks of the phosphate groups, especially 3–5 % $Na_4P_2O_7$ and $Na_5P_3O_{10}$ probably promoted TPS nucleating agent and all phosphate compounds possibly interacted with

TPS through phosphorylation [35].

3.4. Transparency

Fig. 3a shows PBAT/TPS incorporated $Na_4P_2O_7$, $Na_5P_3O_{10}$ and $Na_6(PO_3)_6$ film during blown film extrusion. All films exhibited homogeneous tubular and continuous formation. The transmittance of the films is shown in Fig. 3a. As can be seen, the incorporation of $Na_4P_2O_7$ and $Na_5P_3O_{10}$ decreased light transmittance (increased opacity) due to the network crosslinking by phosphate compounds, which prevented light scattering. Gutiérrez [36] reported that modification of corn starch via phosphorylation crosslinking increased opacity. Conversely, light transmittance increased with increased concentration of $Na_6(PO_3)_6$, which had a cyclic phosphate structure that increased free volume, leading to higher light transmission. Additionally, cyclic phosphate derivatives can form crosslinked structures that can influence the film's morphology and optical properties, where a compact structure can reduce light scattering, leading to improved transparency [15,37]. The results obtained suggested that light transmission was modified by the chemical structures of the phosphate compounds.

3.5. Scanning electron microscopy with energy dispersive X-ray spectroscopy (SEM-EDX)

Surface microstructures of PBAT/TPS containing $Na_4P_2O_7$, $Na_5P_3O_{10}$ and $Na_6(PO_3)_6$ are shown in Fig. 3b. Polymer polarity was the major factor of interfacial adhesion and compatibility of the polymer blends, leading to good polymer properties [38]. PBAT is a more hydrophobic polymer due to the aromatic benzene ring and the hydrocarbon chain, while TPS is a hydrophilic polymer that has high hydroxyl groups. The PBAT/TPS blended film showed phase separation, non-homogeneous structure and rough surface. The rough surface displayed clumps of TPS granules (~10–20 μm) due to incomplete starch melting during the extrusion process [15]. PBAT/TPS films incorporating phosphate

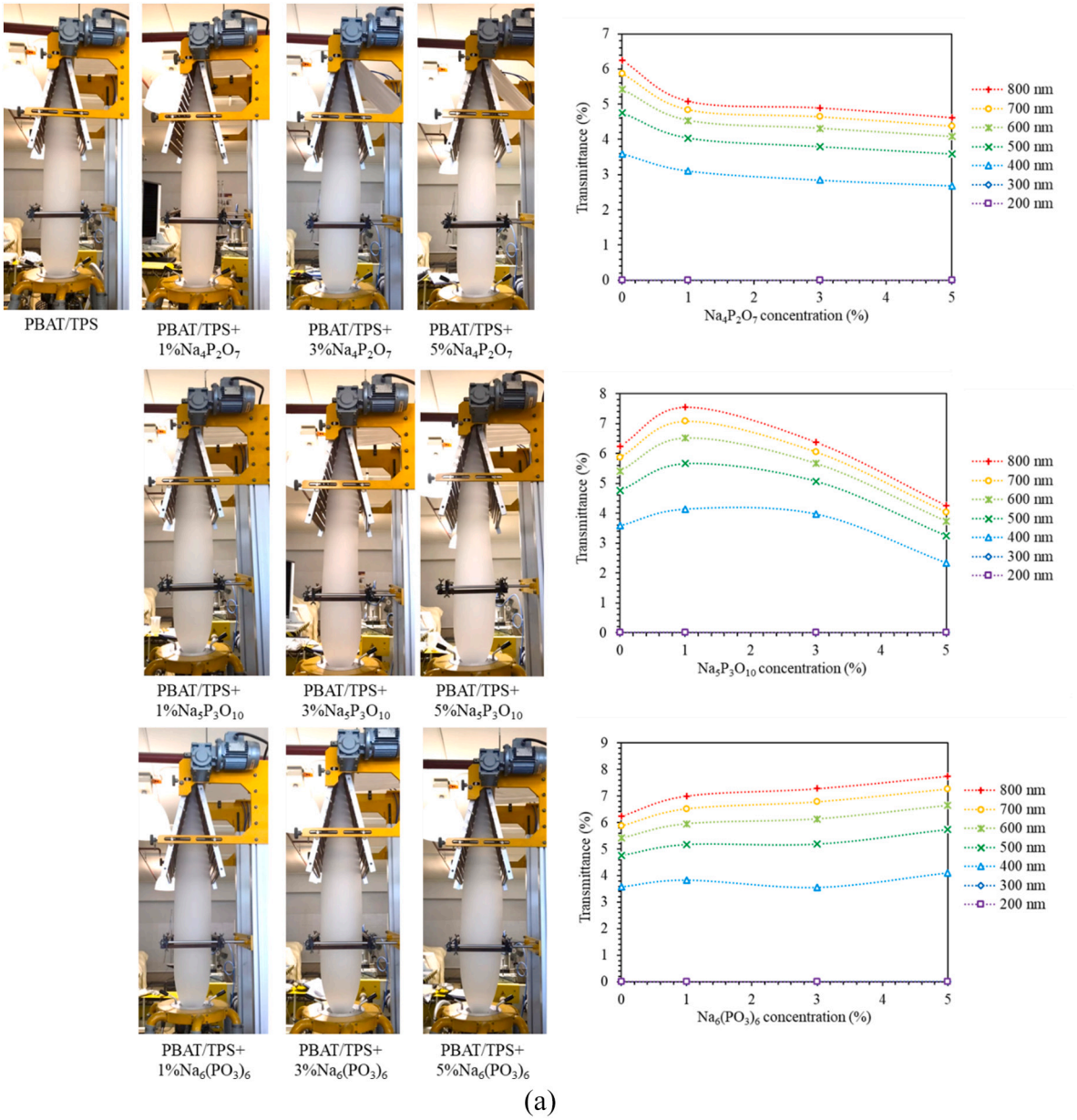

Fig. 3. Morphology; (a) appearance during blown-film extrusion and light transparency, and scanning electron micrographs of (b) surface, (c) cross-section, and (d) AFM surface topography of PBAT/TPS blend films containing tetrasodium pyrophosphate ($Na_4P_2O_7$), sodium tripolyphosphate ($Na_5P_3O_{10}$), and sodium hexametaphosphate ($Na_6(PO_3)_6$) at different ratios (0, 1, 3 and 5 %).

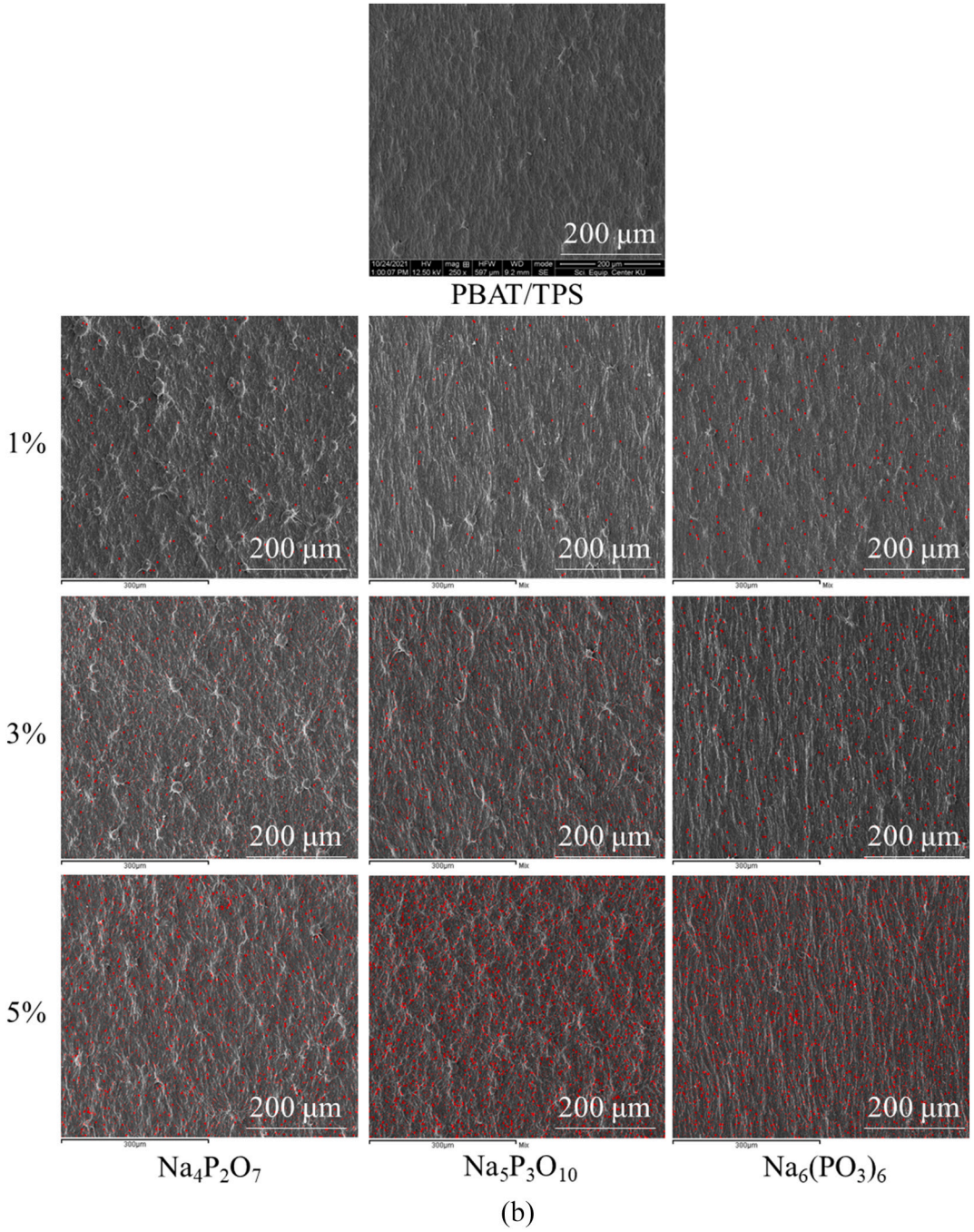

Fig. 3. (*continued*).

compounds formed more TPS agglomeration, while films containing high concentrations of $Na_6(PO_3)_6$ showed reduced size of TPS granules, concurrent with $Na_6(PO_3)_6$ films that displayed a fibrous structure and enhanced co-continuous phases and interconnected TPS structures. The SEM-EDX results shown in Fig. 3b implied good distribution of phosphorus particles in the film matrices (red dots). The number of phosphorus particles increased with increasing concentration up to 5 %, indicating compound aggregation. The clumps increased solid attraction forces, affecting the mechanical and barrier properties of the films.

Cross-sections of PBAT/TPS films are shown in Fig. 3c. The control film showed an immiscible matrix. Increasing phosphate compounds up to 5 % the size of dispersed TPS granules decreased, indicating that phosphate compounds improved TPS granule melting. The $Na_4P_2O_7$ and $Na_5P_3O_{10}$ additions exhibited better-dispersed particles embedded in the matrix with increasing concentration. Incorporation of (1–5 %) $Na_6(PO_3)_6$ was more homogeneous, providing a compatible and denser structure because increasing the phosphate groups (six phosphate) effectively modified the starch structure and eliminated starch granules. Thus, this phosphate-starch modification suggested that $Na_6(PO_3)_6$ gave a more compatible matrix. The results shown are compatible with the emulsifying, surfactant, and dispersing capabilities of $Na_6(PO_3)_6$, commonly utilized in the food and chemical industries [14]. Phosphate addition increased hydrophobicity and enhanced hydrophobic interaction with PBAT, while $Na_6(PO_3)_6$ showed the highest potential to improve compatibility between PBAT and TPS blended films.

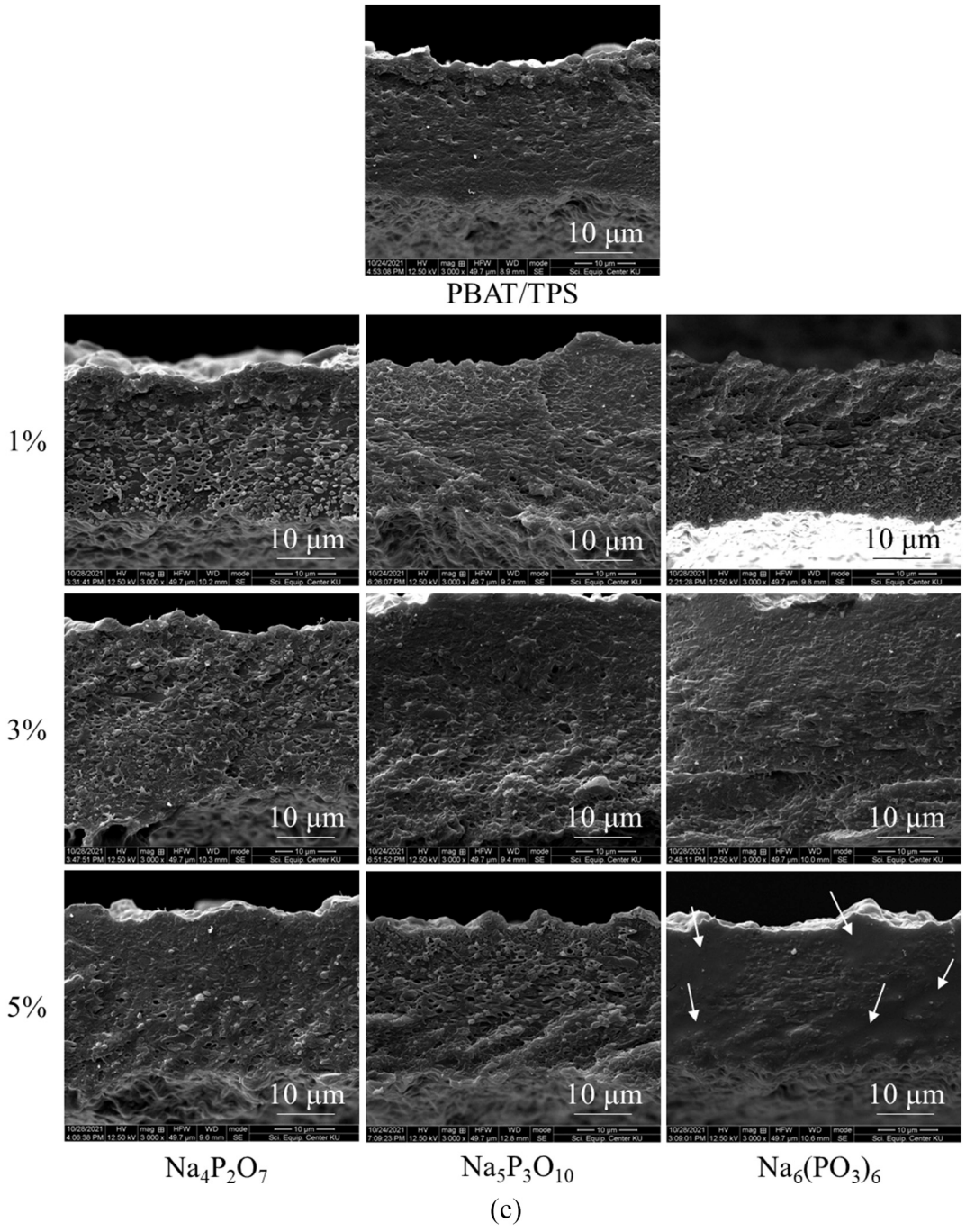

Fig. 3. (*continued*).

3.6. Atomic force microscopy (AFM)

Topographic images in Fig. 3d show rough surfaces and non-homogeneous structures in PBAT/TPS films. The incorporation of phosphate compounds modified the film surface. $Na_4P_2O_7$ and $Na_5P_3O_{10}$ exhibited dispersed particles, reducing starch granule agglomeration. The 5 % $Na_6(PO_3)_6$ film showed the smoothest and most homogeneous surface, which improved the strength of the films [1,15]. These results indicated that $Na_4P_2O_7$, $Na_5P_3O_{10}$ and $Na_6(PO_3)_6$ influenced immiscibility of the bioplastic blended film and enhanced melting of TPS granules and TPS dispersion. $Na_6(PO_3)_6$ was the most effective compatibilizer for PBAT/TPS blends.

3.7. Differential scanning calorimetry (DSC)

DSC thermograms of PBAT/TPS containing $Na_4P_2O_7$, $Na_5P_3O_{10}$ and $Na_6(PO_3)_6$ provided thermal behaviors namely crystalline melting temperature (T_m) and re-crystallization temperature (T_c). Fig. 4a shows broader areas at 52 °C and 109 °C related to T_m of polybutylene adipate (PBA) and rigid polybutylene terephthalate (PBT) segments in PBAT, respectively. Both segments were slightly modified at higher temperature (~ 111 °C) because the incorporated phosphate compounds enhanced the molecular arrangements in the polymer structure [38,39]. A temperature of 174.17 °C related to T_m of PBAT/TPS blended matrices and also provided melting enthalpy (ΔH_m) (data in Supplement 2). Incorporated phosphate films, T_m and ΔH_m were modified, while T_m of all phosphates (1 %) shifted to a higher temperature than the control

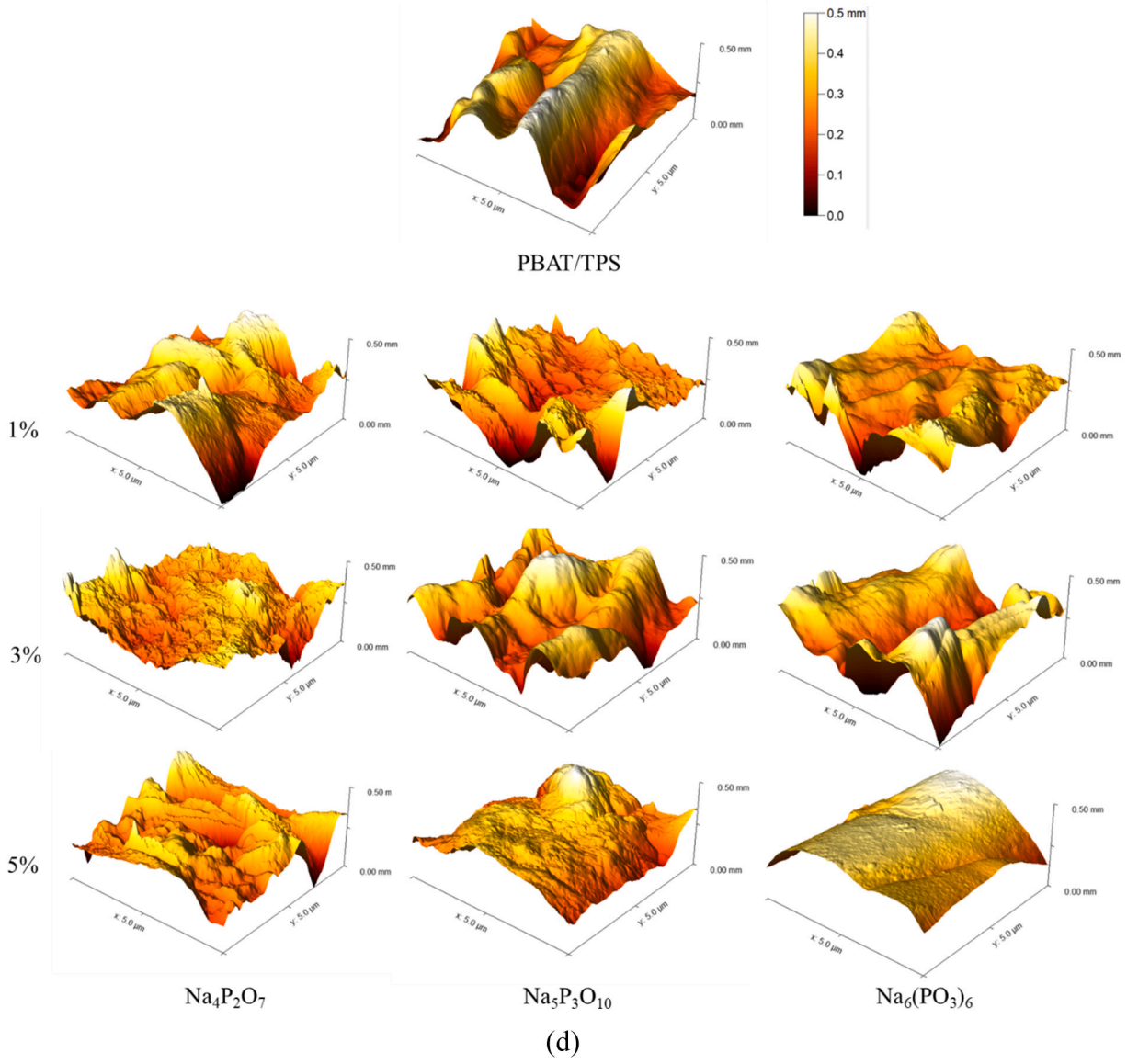

Fig. 3. (*continued*).

film due to the formation of ordered PBAT/TPS, corresponding with the XRD result. Increasing concentrations of $Na_4P_2O_7$ and $Na_6(PO_3)_6$ led to lower T_m because the phosphate compounds destroyed the hydrogen bonds, while ΔH_m values decreased. Woggum, Sirivongpaisal, & Wittaya [26] demonstrated that ΔH_m decreased as a result of crosslinking reagents that disrupted the molecular ordered starch structure at the double helical of amylopectin. The results indicated that when the ordered starch segments reduced a weaker bonding in the starch molecules occurred by phosphate substitution. The T_c of PBAT/TPS films, shown in Fig. 4b, confirms the crystalline formation of the matrix. The T_c of PBAT/TPS film was 74.83 °C and T_c values of $Na_4P_2O_7$ and $Na_5P_3O_{10}$ films slightly shifted to lower temperatures (~73–74 °C) (Supplement 2). $Na_6(PO_3)_6$ exhibited the lowest T_c depending on concentration because $Na_6(PO_3)_6$ plasticized starch in PBAT/TPS matrices that enhanced the mobility in an amorphous phase [4,39]. The enthalpy of crystallization (ΔHc) relates to the amount of crystallization and confirmed that phosphate compounds promoted the amorphous-rich phase in PBAT/TPS blended film at increasing concentrations. Therefore, the addition of phosphate compounds effectively influenced thermal transitions of the PBAT/TPS films by destroying the ordered structure.

3.8. Thermogravimetric analysis (TGA)

The thermal degradation profiles of PBAT/TPS films indicated the thermal stability of biodegradable film, determined by TGA as mass weight loss (Fig. 4c) and 1st derivative TGA curve (Fig. 4d). The TGA curve occurred in four steps. The first mass loss was below 100 °C due to loss of adsorbed water (~10 %). The second mass loss occurred between 200 and 250 °C, with other steps between 250 and 350 °C and 350 and 450 °C attributed to glycerol, TPS and PBAT components, respectively [4,38]. The temperature range between 50 and 150 °C showed that phosphate compounds improved water stability, leading to higher water evaporation temperature depending on concentration, especially in $Na_6(PO_3)_6$. Phosphate compounds have an oxygen atom that easily forms H-bonding with water molecules (P—O— and –O–H). Interaction between glycerol-phosphate compounds shown in the second step had the same trend as water vaporization. The TPS peak (250–350 °C) exhibited the degradation temperature (T_d) of the TPS phase, while incorporating phosphate compounds gave lower T_d than the control film, depending on concentration, because the hydroxyl groups in starch molecules were destroyed by phosphate groups, leading to weaker bonding. These peaks in phosphate films, especially $Na_6(PO_3)_6$, films,

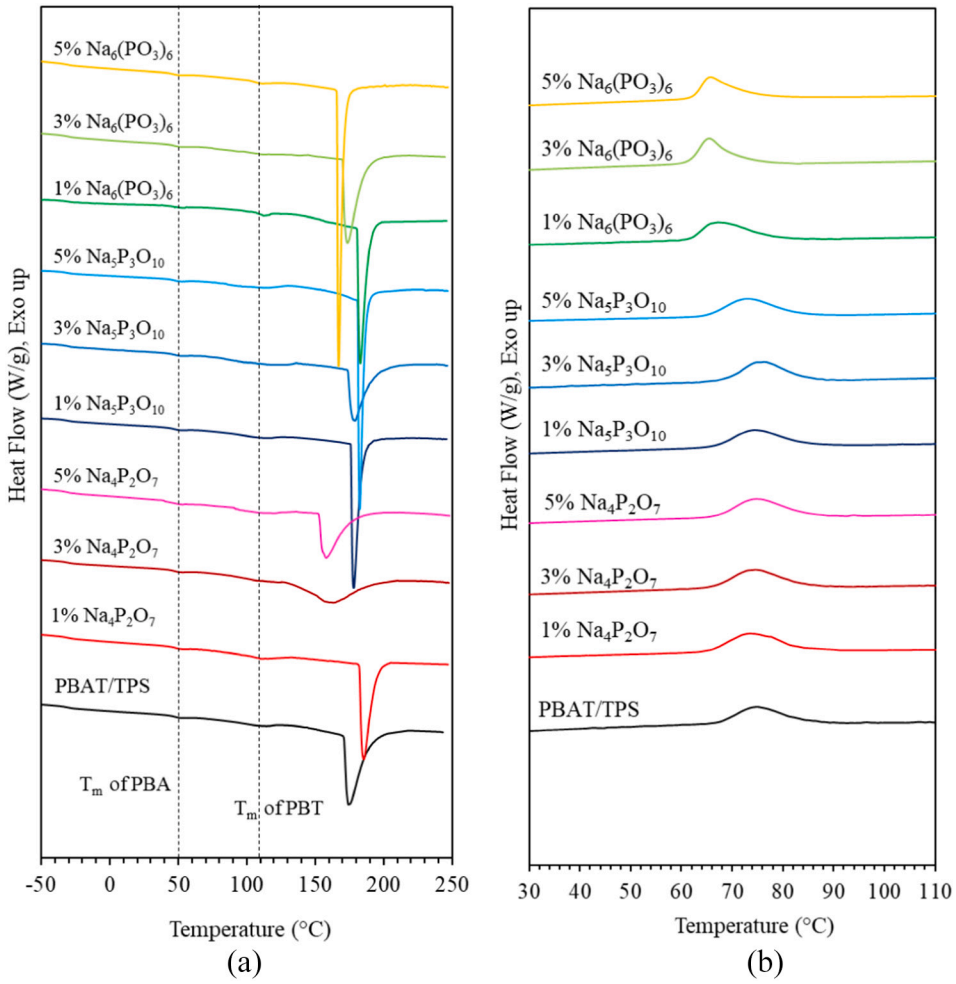

Fig. 4. Thermal properties; differential scanning calorimetry (DSC) as determined by (a) heating curve, (b) cooling curve, and thermal degradations as (c) TGA curve, (d) 1st derivative TGA, (e) storage modulus and (f) relaxation temperature using DMTA of PBAT/TPS blend films containing tetrasodium pyrophosphate ($Na_4P_2O_7$), sodium tripolyphosphate ($Na_5P_3O_{10}$), and sodium hexametaphosphate ($Na_6(PO_3)_6$) at different ratios (0, 1, 3 and 5 %).

demonstrated merging with the glycerol rich phase. Phosphate TPS-glycerol interaction as high plasticization reduced thermal stability in the starch phase. The PBAT phase (350–450 °C) showed a peak at 407 °C for the control film, while increasing phosphate concentration increased the T_d of PBAT because PBAT-phosphate interaction enhanced the ordered PBAT structure. Phosphate compounds acted as TPS nucleating agents in the PBAT matrix, as shown by the FTIR results. Phosphate compounds acted as plasticizing and nucleating agents for biodegradable polymers. The addition of $Na_4P_2O_7$, $Na_5P_3O_{10}$, and $Na_6(PO_3)_6$ interacted with and modified the TPS and PBAT structures, causing a shift in Td.

3.9. Dynamic mechanical thermal analysis (DMTA)

The dynamic mechanical behaviors of the material as the storage modulus (E') and the loss factor (tan δ) of PBAT/TPS blended films are shown in Fig. 4e and f. Various frequencies (5, 10 and 20 Hz) as a function of temperature indicated polymer chain movement. The dynamic mechanical behavior of all samples was frequency dependent. Storage modulus decreased with increasing temperature and was sensitive to polymer molecule motion and chain structure [10,23]. The storage modulus relates to the storage energy under molecular deformation, indicating material stiffness. PBAT/TPS film showed that the inflection point of the storage modulus rapidly decreased below −40 °C, implying that the materials transformed into a rubbery state when heated due to increased molecular mobility. This was attributed to the interaction between the glycerol-rich TPS phase. Incorporating phosphate compounds into PBAT/TPS film changed the storage modulus from the control film. These results indicated a limited polymer chain mobility, strong chemical interaction (H-bonding) and crosslinking with phosphate compounds [10].

Fig. 4f shows the peak of tan δ associated with the energy dissipation capacity of the material, and corresponding to the storage modulus curve. The peak of tan δ indicated the relaxation temperature of the PBAT/TPS films. Small and larger peaks at −80 to −40 °C and − 40 to 10 °C were attributed to the relaxation temperature of the glycerol-rich TPS phase and PBAT matrix, respectively. The PBAT/TPS film exhibited two main relaxations due to phase separation and immiscibility of the polymer blends. When incorporating phosphate compounds, both peaks slightly merged indicating interaction between the phosphate compounds and the TPS/PBAT phase. Bonding between glycerol, phosphate compounds and starch gave higher levels of amorphous starch leading to increase relaxation temperature. The relaxation temperature increased with increasing phosphate concentration because bulk polymers from the phosphate compounds interacted with the PBAT and TPS phases, providing amorphous polymers [5,10]. Phosphate groups formed covalent bonds with starch (P-O-C), improving the intermolecular interaction of the polymer, which restricted molecular mobility and resulted

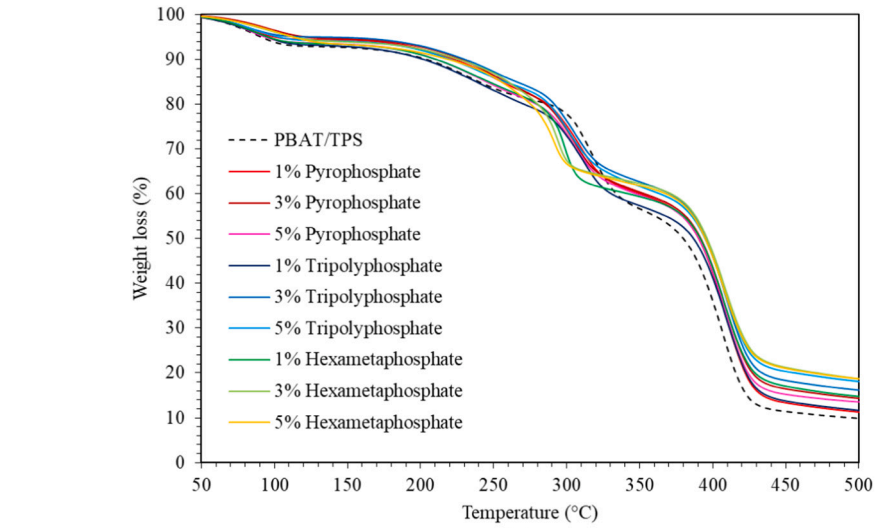

(c)

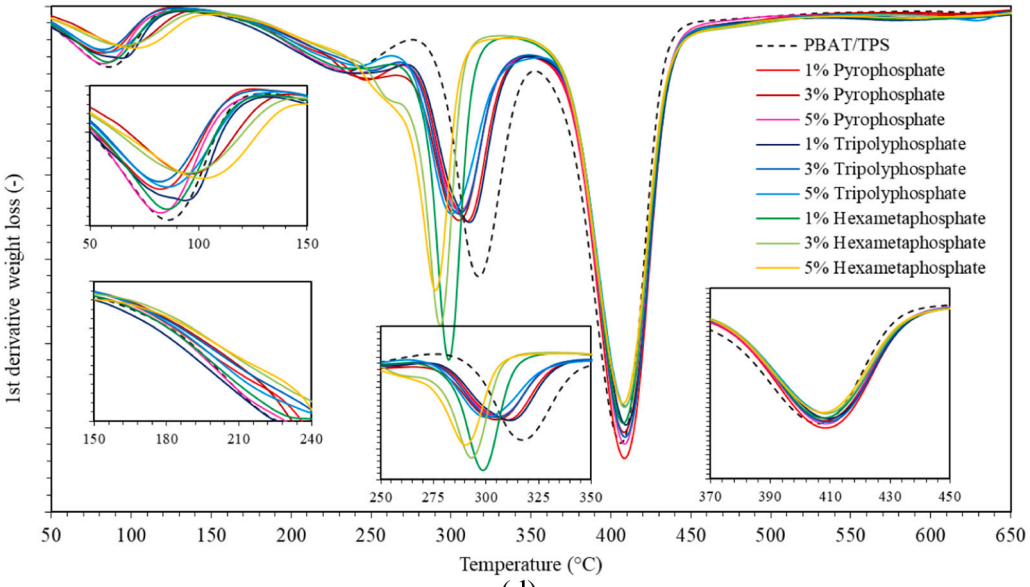

(d)

Fig. 4. (*continued*).

in a higher relaxation temperature due to the increased amount of amorphous material. Thus, the phosphate compounds strongly influenced molecular motion and enhanced the stiffness of the material.

3.10. Mechanical properties

Fig. 5 shows the static mechanical properties, namely strength and flexibility of PBAT/TPS films. The control film exhibited the highest TS, while incorporating $Na_4P_2O_7$, $Na_5P_3O_{10}$ and $Na_6(PO_3)_6$ significantly decreased TS because the phosphate compounds disrupted hydrogen bonding and modified the starch granules. Introducing modifier molecules into amorphous phase regions significantly decreases mechanical strength [1,35]. Mechanical strength depends on matrix immiscibility. The SEM images demonstrated fine clumps and non-homogeneous microstructure, with decreasing strength depending on the phosphate concentrations. EB decreased with addition of phosphate compounds. Samples containing $Na_4P_2O_7$ and $Na_5P_3O_{10}$ showed significantly decreased flexibility because both compounds restricted molecular mobility in the polymer chain, providing less flexible material and increasing stiffness related to the thermal behavior. The 3 % $Na_6(PO_3)_6$ sample had the highest EB value caused by oxygen atoms that easily interacted with water molecules to enhance plasticization and miscibility of the polymer blends. Increasing $Na_6(PO_3)_6$ to 5 % significantly reduced EB compared to the control film, resulting in the amorphous domain of PBAT/TPS films. Addition of $Na_4P_2O_7$, $Na_5P_3O_{10}$ and $Na_6(PO_3)_6$ effectively influenced mechanical properties, due to the enhanced amorphous regions and limited chain mobility of the polymer blends.

3.11. Seal strength

Seal strength was interpreted as the peelability of interfacial adhesion between the surfaces of PBAT/TPS film to avoid packaging delamination, as shown in Fig. 5. Seal strength depends on interfacial melting temperature, chain diffusion rate, melt strength, entanglement and crystallization rate [40]. PBAT/TPS film containing 1 % phosphate compounds displayed statistically significant ($\alpha < 0.05$) enhancement in interfacial adhesion of PBAT/TPS film (control) because the phosphate groups disrupted the starch structure, according to the FTIR results. Phosphate compounds promoted starch modification, which enhanced

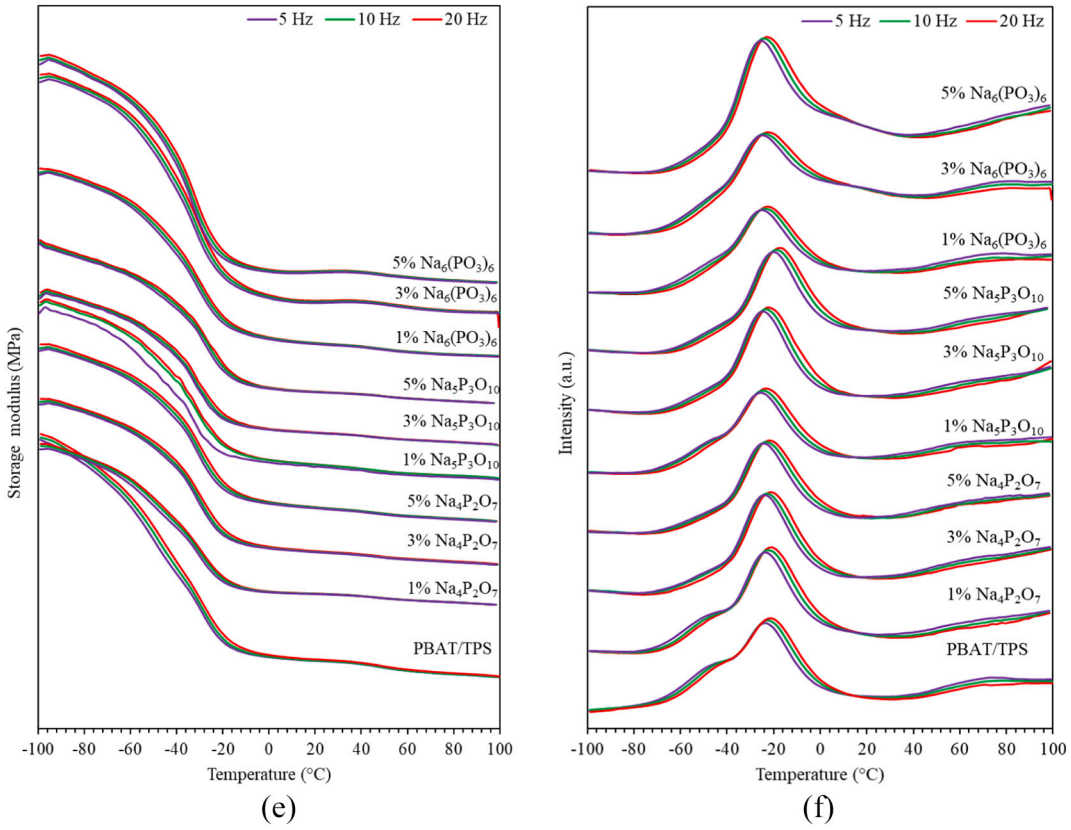

Fig. 4. (*continued*).

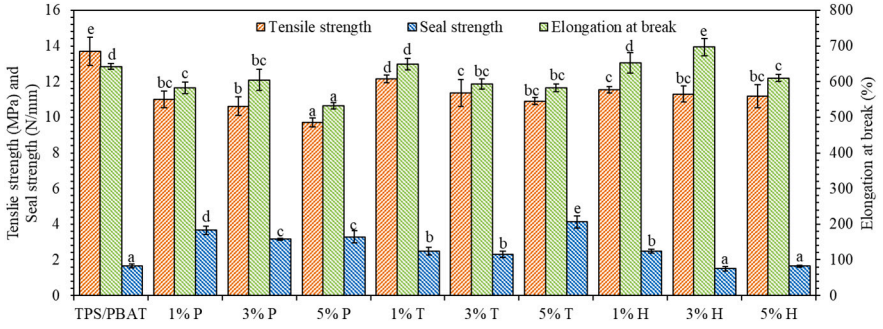

Fig. 5. Mechanical properties; tensile strength, elongation at break, and seal strength of PBAT/TPS blend films containing tetrasodium pyrophosphate ($Na_4P_2O_7$) as P, sodium tripolyphosphate ($Na_5P_3O_{10}$) as T, and sodium hexametaphosphate ($Na_6(PO_3)_6$) as H at different ratios (0, 1, 3 and 5 %).

bonding strength and chain interaction. Increasing the concentration of $Na_5P_3O_{10}$ significantly improved seal strength. $Na_5P_3O_{10}$ was the most effective, in good agreement with Zhang, Li & Wang [11] and López, Lecot, Zaritzky & García [41]. However, increasing the concentrations of $Na_4P_2O_7$ and $Na_6(PO_3)_6$ decreased seal strength. Both compounds enhanced a smooth surface, probably leading to reduced surface energy and adhesion performance of the material. Incorporating phosphate compounds reduced recrystallization and increased the amorphous phase, which restricted entanglement and chain mobility, thus providing a higher relaxation temperature and decreasing heat transfer efficiency in the seal strength.

3.12. Surface wettability

The PBAT/TPS surface wetting was determined by the contact angle (CA) at the film surface (Fig. 6). Important factors influencing CA values are surface roughness and heterogeneity consisting of hydrophobic and hydrophilic regions, particle shape, and particle size [15,42]. PBAT/TPS films exhibited hydrophilic surfaces (below 90°). Films containing 1–3 % $Na_5P_3O_{10}$ and 1–5 % $Na_6(PO_3)_6$ showed reduced CA because the phosphate groups enhanced hydrophilicity. Phosphate groups consist of one phosphorus atom attached to four oxygen atoms by a covalent bond, while $Na_5P_3O_{10}$ and $Na_6(PO_3)_6$ have three and six phosphate groups, respectively and easily interact with water molecules depending on the number of phosphate groups, giving high hydrophilic properties. $Na_4P_2O_7$ addition resulted in a rough surface with fine clumps, correlating with the SEM image, leading to significantly improved CA. The addition of phosphate compounds modified the surface wetting by changing the chemical structure and microstructure of the matrix surface.

3.13. Barrier properties

Fig. 6 presents the barrier properties of PBAT/TPS films as water

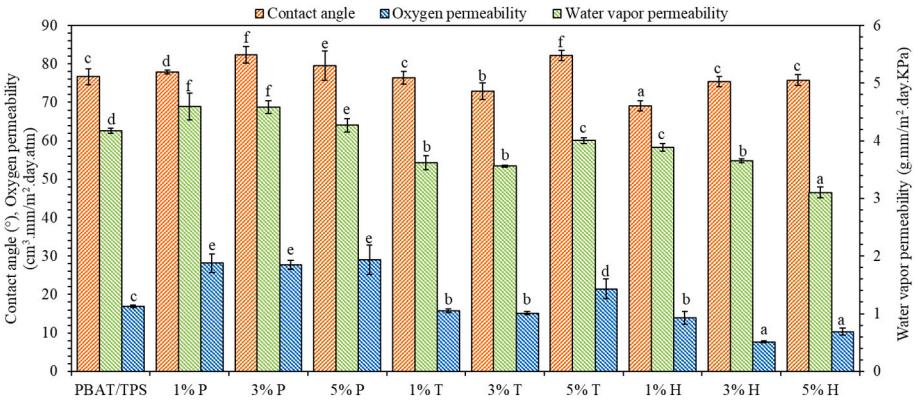

Fig. 6. Barrier properties; contact angle (CA), water vapor permeability (WVP), and oxygen permeability (OP) of PBAT/TPS blend films containing tetrasodium pyrophosphate ($Na_4P_2O_7$) as P, sodium tripolyphosphate ($Na_5P_3O_{10}$) as T, and sodium hexametaphosphate ($Na_6(PO_3)_6$) as H at different ratios (0, 1, 3 and 5 %).

vapor permeability (WVP) and oxygen permeability (OP) depending on absorption, diffusion and desorption processes which are necessary for food packaging. Polymer and permeant characteristics are important factors that include material affinity, crystallinity, orientation, relaxation transition, concentration, functional groups and carbon chain length, which impact the mass transport of vapor through the matrices [28]. The WVP and OP values of the PBAT/TPS films had similar tendencies. Incorporation of $Na_6(PO_3)_6$ up to 3–5 % exhibited excellent barrier properties with lowest WVP and OP values at 3.10 g.mm/m^2.day.KPa and 7.69–10.34 cm^3.mm/m^2.day.atm, respectively. The $Na_6(PO_3)_6$ at increasing concentration gave a more homogeneous and denser structure that prevented mass transition diffusion, resulting in a reduced permeability, while films containing $Na_4P_2O_7$ had a significantly increased permeability because phosphate compound esters are symmetrical, with tetrahedral shape as a non-polar characteristic, giving high OP values. The $Na_4P_2O_7$ films provided high WVP with hydrophilic surfaces. The oxygen atoms in the structure easily reacted with water molecules, enhancing water absorption and diffusion. When adding $Na_5P_3O_{10}$, the film permeability decreased, owing to the strong interaction between phosphate and the PBAT/TPS matrix. $Na_5P_3O_{10}$ addition provided a high amorphous region and high glass transition temperature that reduced free volume and molecular mobility, thereby reducing the permeability. These results suggested that permeability of the PBAT/TPS films was modified by the polymer chemical structure, heterogeneity and microstructure of the matrices.

3.14. Antimicrobial activity of the PBAT/TPS films

The PBAT/TPS containing phosphate compounds was studied with *E. coli* as a pathogenic organism because it contaminated fresh produces and was found in fresh produces causing implicated in outbreaks of foodborne illness and contaminated fresh produces [43]. Laorenza & Harnkarnsujarit [17] reported that the turbidity measurement determined the optical density levels related to the microbial growth and concentration using the liquid broth technique. Fig. 7a shows the optical density during incubate 5 days. The results indicated the microbial growth profile corresponds to the number of *E. coli* colonies (Fig. 7b). The trend of optical density in the control film rapidly increased with dependence on time ($y = 0.0035 \times ^2 + 0.0645\times$ - 0.0029, $R^2 = 0.9979$) while PBAT/TPS with phosphate compounds slightly increased, indicating all phosphate compounds delayed the microbial growth. Films containing $Na_4P_2O_7$ had higher optical density values than $Na_5P_3O_{10}$ and $Na_6(PO_3)_6$ probably due to the number of phosphorus atoms in the phosphate chains. The higher phosphate groups caused the lag-time prolongations in *E. coli* which decreased the specific growth rate and extended the generation time [44]. The number of *E. coli* reduced proportional to the optical density values. PBAT/TPS containing phosphate compounds had lower numbers of colonies than control film. Increasing

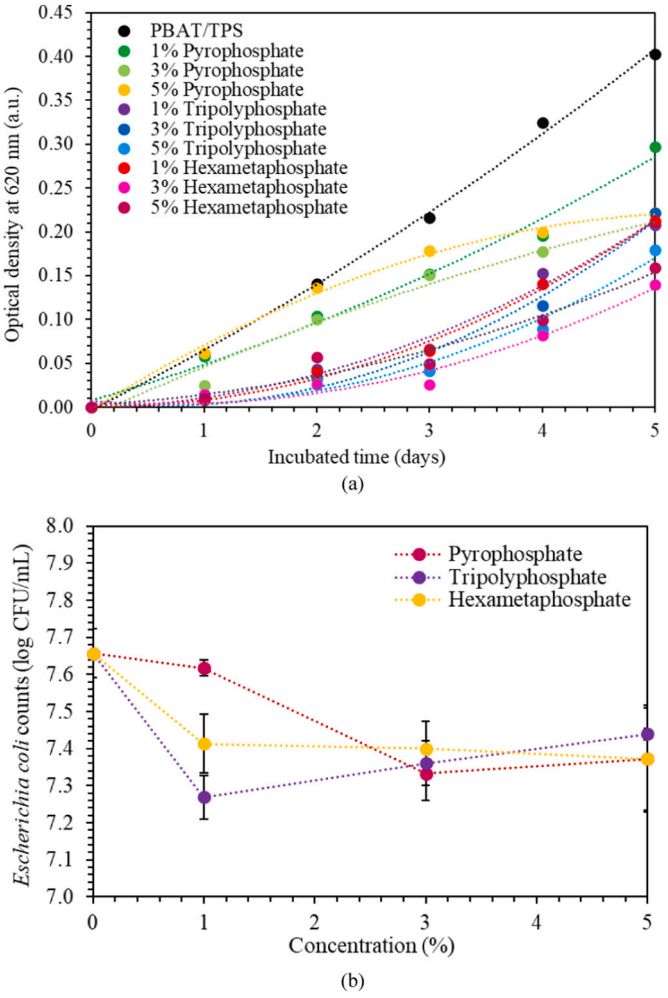

Fig. 7. (a) The optical density and (b) the number of *E. coli* colonies of PBAT/TPS blend films containing tetrasodium pyrophosphate ($Na_4P_2O_7$), sodium tripolyphosphate ($Na_5P_3O_{10}$), and sodium hexametaphosphate ($Na_6(PO_3)_6$) at different ratios (0, 1, 3 and 5 %).

$Na_4P_2O_7$, $Na_5P_3O_{10}$ and $Na_6(PO_3)_6$ phosphate concentration (1–5 %) showed insignificant *E. coli* colonies maybe due to phosphate groups enhanced the lag-time prolongations and did not affect the number of microbials. Therefore, all phosphate compounds incorporated PBAT/TPS film acting as the antimicrobial agents which it influenced the bacterial cell by the chelation of metal ions.

4. Conclusions

Incorporation of $Na_4P_2O_7$, $Na_5P_3O_{10}$ and $Na_6(PO_3)_6$ at different concentrations (1–5 %) into PBAT/TPS blended films produced by blown-film extrusion modified the chemical polymeric matrix. Phosphate-starch modification induced by covalent bonding (P–O–C), enhanced the amorphous fraction. Phosphate substitution primarily occurred at the C-6 position of the anhydroglucose unit, leading to various degrees of starch phosphorylation. In addition, $Na_4P_2O_7$, $Na_5P_3O_{10}$ and $Na_6(PO_3)_6$ destroyed the α-1,6 glycosidic linkages between the starch chains during extrusion, as confirmed by FTIR and ^1H NMR. The crystallinity of the PBAT/TPS films reduced because cross-linking networks provided covalent bonds between the polymer chains that restricted molecular mobility. Addition of phosphate compounds increased hydrophobicity and enhanced hydrophobic interaction with PBAT, thereby increasing compatibility between PBAT and the TPS matrix. Films containing phosphate compounds were less flexible, with increased stiffness related to the thermal transition. Cyclic polymers in the phosphate compounds interacted with PBAT and TPS phases, providing amorphous polymers and increasing relaxation temperature. Interfacial adhesion of the PBAT/TPS films resulted in improved peel/seal strength, while wettability and permeability were modified by the polymer structure, heterogeneity and microstructure. The addition of $Na_4P_2O_7$, $Na_5P_3O_{10}$ and $Na_6(PO_3)_6$ influenced water vapor and oxygen permeability. The results obtained demonstrated that phosphate derivatives modify cassava starch via phosphate-starch interaction and also impact the physicochemical, morphological and thermal properties. Findings suggested the sustainable phosphate PBAT/TPS biodegradable packaging effectively sustainable packaging with effective functionality and potential to slow down microbial growth. However, the blend of PBAT/TPS with phosphate derivatives may result in low hydrophobicity and mechanical properties. Future research should focus on optimizing the formulation and processing conditions to further enhance the properties of these biodegradable films and address potential limitations, such as reduced flexibility and hydrophobicity. By incorporating additional additives or modifying the processing techniques, it is possible to develop sustainable packaging materials with properties comparable to conventional plastic films.

CRediT authorship contribution statement

Phanwipa Wongphan: Writing – review & editing, Writing – original draft, Methodology, Investigation, Formal analysis, Data curation, Conceptualization. **Cristina Nerín:** Writing – review & editing. **Nathdanai Harnkarnsujarit:** Writing – review & editing, Writing – original draft, Validation, Supervision, Methodology, Funding acquisition, Conceptualization.

Declaration of competing interest

The authors declare that they have no known competing financial interests or personal relationships that could have appeared to influence the work reported in this paper.

Acknowledgements

This research project was supported by the National Research Council of Thailand (NRCT), Contract No. N41A640190 (The Royal Golden Jubilee Ph.D. Program), Contract No. N41A640082 and Kasetsart University Research and Development Institute (KURDI) FF(KU) 8.67.

Appendix A. Supplementary data

Supplementary data to this article can be found online at https://doi.org/10.1016/j.ijbiomac.2024.137906.

Data availability

The authors are unable or have chosen not to specify which data has been used.

References

[1] C.C. Chang, B.M. Trinh, T.H. Mekonnen, Robust multiphase and multilayer starch/polymer (TPS/PBAT) film with simultaneous oxygen/moisture barrier properties, J. Colloid Interface Sci. 593 (2021) 290–303.
[2] J. Jian, Z. Xiangbin, H. Xianbo, An overview on synthesis, properties and applications of poly(butylene-adipate-co-terephthalate)–PBAT, Advanced Industrial and Engineering Polymer Research 3 (1) (2020) 19–26, https://doi.org/10.1016/j.aiepr.2020.01.001.
[3] S. Roy, T. Ghosh, W. Zhang, J.-W. Rhim, Recent progress in PBAT-based films and food packaging applications: a mini-review, Food Chem. 437 (2024) 137822.
[4] J. Bai, H. Pei, X. Zhou, X. Xie, Reactive compatibilization and properties of low-cost and high-performance PBAT/thermoplastic starch blends, Eur. Polym. J. 143 (2021) 110198.
[5] J.B.A. da Silva, R.E.S. Bretas, A.A. Lucas, J. Marini, A.B. da Silva, J.S. Santana, F. V. Pereira, J.I. Druzian, Rheological, mechanical, thermal, and morphological properties of blends poly (butylene adipate-co-terephthalate), thermoplastic starch, and cellulose nanoparticles, Polym. Eng. Sci. 60 (7) (2020) 1482–1493.
[6] A.R. de Matos Costa, A. Crocitti, L. Hecker de Carvalho, S.C. Carroccio, P. Cerruti, G. Santagata, Properties of biodegradable films based on poly (butylene succinate) (PBS) and poly (butylene adipate-co-terephthalate)(PBAT) blends, Polymers 12 (10) (2020) 2317.
[7] T. Woggum, P. Sirivongpaisal, T. Wittaya, Properties and characteristics of dual-modified rice starch based biodegradable films, Int. J. Biol. Macromol. 67 (2014) 490–502.
[8] K. Wadaugsorn, T. Panrong, P. Wongphan, N. Harnkarnsujarit, Plasticized hydroxypropyl cassava starch blended PBAT for improved clarity blown films: morphology and properties, Ind. Crop. Prod. 176 (2022) 114311.
[9] P. Wongphan, C. Nerin, N. Harnkarnsujarit, Enhanced compatibility and functionality of thermoplastic cassava starch blended PBAT blown films with erythorbate and nitrite, Food Chem. 420 (2023) 136107, https://doi.org/10.1016/j.foodchem.2023.136107.
[10] H. Peidayesh, A. Heydari, K. Mosnackova, I. Chodak, In situ dual crosslinking strategy to improve the physico-chemical properties of thermoplastic starch, Carbohydr. Polym. 269 (2021) 118250, https://doi.org/10.1016/j.carbpol.2021.118250.
[11] J. Zhang, A. Li, A. Wang, Study on superabsorbent composite. VI. Preparation, characterization and swelling behaviors of starch phosphate-graft-acrylamide/attapulgite superabsorbent composite, Carbohydr. Polym. 65 (2) (2006) 150–158.
[12] M. Wei, Y. Liu, B. Liu, X. Lv, P. Sun, Z. Zhang, F. Zhang, S. Yin, Z. Liu, Preparation and application of starch phosphate with a low degree of substitution, Phosphorus Sulfur Silicon Relat. Elem. 186 (4) (2011) 974–982.
[13] Y. Hu, L. Zhang, Y. Yi, I. Solangi, L. Zan, J. Zhu, Effects of sodium hexametaphosphate, sodium tripolyphosphate and sodium pyrophosphate on the ultrastructure of beef myofibrillar proteins investigated with atomic force microscopy, Food Chem. 338 (2021) 128146, https://doi.org/10.1016/j.foodchem.2020.128146.
[14] O.M. Power, M.A. Fenelon, J.A. O'Mahony, N.A. McCarthy, Influence of sodium hexametaphosphate addition on the functional properties of milk protein concentrate solutions containing transglutaminase cross-linked proteins, Int. Dairy J. 104 (2020) 104641.
[15] K. Wadaugsorn, T. Panrong, P. Wongphan, N. Harnkarnsujarit, Plasticized hydroxypropyl cassava starch blended PBAT for improved clarity blown films: morphology and properties, Ind. Crop. Prod. 176 (2022), https://doi.org/10.1016/j.indcrop.2021.114311.
[16] N. Bumbudsanpharoke, P. Wongphan, K. Promhuad, P. Leelaphiwat, N. Harnkarnsujarit, Morphology and permeability of bio-based poly(butylene adipate-co-terephthalate) (PBAT), poly(butylene succinate) (PBS) and linear low-density polyethylene (LLDPE) blend films control shelf-life of packaged bread, Food Control 132 (2022), https://doi.org/10.1016/j.foodcont.2021.108541.
[17] Y. Laorenza, N. Harnkarnsujarit, Ginger oil and lime peel oil loaded PBAT/PLA via cast-extrusion as shrimp active packaging: microbial and melanosis inhibition, Food Packag. Shelf Life 38 (2023), https://doi.org/10.1016/j.fpsl.2023.101116.
[18] A.O. Ashogbon, E.T. Akintayo, Recent trend in the physical and chemical modification of starches from different botanical sources: a review, Starch-Stärke 66 (1–2) (2014) 41–57.
[19] I. Dankar, A. Haddarah, F.E. Omar, M. Pujolà, F. Sepulcre, Characterization of food additive-potato starch complexes by FTIR and X-ray diffraction, Food Chem. 260 (2018) 7–12.
[20] J.L. Koenig, Spectroscopy of Polymers, Elsevier, 1999.
[21] L.R. Antunes, G.L. Breitenbach, M.C.G. Pellá, J. Caetano, D.C. Dragunski, Electrospun poly (lactic acid)(PLA)/poly (butylene adipate-co-terephthalate) (PBAT) nanofibers for the controlled release of cilostazol, Int. J. Biol. Macromol. 182 (2021) 333–342.
[22] Y. Fourati, Q. Tarrés, M. Delgado-Aguilar, P. Mutjé, S. Boufi, Cellulose nanofibrils reinforced PBAT/TPS blends: mechanical and rheological properties, Int. J. Biol. Macromol. 183 (2021) 267–275.
[23] P. Leelaphiwat, C. Pechprankan, P. Siripho, N. Bumbudsanpharoke, N. Harnkarnsujarit, Effects of nisin and EDTA on morphology and properties of

thermoplastic starch and PBAT biodegradable films for meat packaging, Food Chem. 369 (2022) 130956, https://doi.org/10.1016/j.foodchem.2021.130956.
[24] S. Yang, S. Dhital, M.-N. Zhang, J. Wang, Z.-G. Chen, Structural, gelatinization, and rheological properties of heat-moisture treated potato starch with added salt and its application in potato starch noodles, Food Hydrocoll. 131 (2022), https://doi.org/10.1016/j.foodhyd.2022.107802.
[25] P.F. Duckworth, S.E. Maddocks, S.S. Rahatekar, M.E. Barbour, Alginate films augmented with chlorhexidine hexametaphosphate particles provide sustained antimicrobial properties for application in wound care, J. Mater. Sci. Mater. Med. 31 (3) (2020) 33.
[26] T. Woggum, P. Sirivongpaisal, T. Wittaya, Properties and characteristics of dual-modified rice starch based biodegradable films, Int. J. Biol. Macromol. 67 (2014) 490–502, https://doi.org/10.1016/j.ijbiomac.2014.03.029.
[27] Y. Ding, B. Lu, P. Wang, G. Wang, J. Ji, PLA-PBAT-PLA tri-block copolymers: effective compatibilizers for promotion of the mechanical and rheological properties of PLA/PBAT blends, Polym. Degrad. Stab. 147 (2018) 41–48.
[28] B.M. Trinh, C.C. Chang, T.H. Mekonnen, Facile fabrication of thermoplastic starch/poly (lactic acid) multilayer films with superior gas and moisture barrier properties, Polymer 223 (2021) 123679.
[29] H. Kono, H. Hashimoto, Y. Shimizu, NMR characterization of cellulose acetate: chemical shift assignments, substituent effects, and chemical shift additivity, Carbohydr. Polym. 118 (2015) 91–100, https://doi.org/10.1016/j.carbpol.2014.11.004.
[30] M.P. Williamson, Using chemical shift perturbation to characterise ligand binding, Prog. Nucl. Magn. Reson. Spectrosc. 73 (2013) 1–16.
[31] M.E. El-Naggar, M.H. El-Rafie, M.A. El-sheikh, G.S. El-Feky, A. Hebeish, Synthesis, characterization, release kinetics and toxicity profile of drug-loaded starch nanoparticles, Int. J. Biol. Macromol. 81 (2015) 718–729, https://doi.org/10.1016/j.ijbiomac.2015.09.005.
[32] Y. Laorenza, N. Harnkarnsujarit, Surface adhesion and physical properties of modified TPS and PBAT multilayer film, Food Packag. Shelf Life 44 (2024) 101312.
[33] H. Peidayesh, Z. Ahmadi, H.A. Khonakdar, M. Abdouss, I. Chodák, Fabrication and properties of thermoplastic starch/montmorillonite composite using dialdehyde starch as a crosslinker, Polym. Int. 69 (3) (2020) 317–327.
[34] L. Ren, Y. Fu, Y. Chang, M. Jiang, J. Tong, J. Zhou, Performance improvement of starch films reinforced with starch nanocrystals (SNCs) modified by cross-linking, Starch-Stärke 69 (1–2) (2017) 1600025.
[35] W. Liu, S. Liu, Z. Wang, B. Dai, J. Liu, Y. Chen, G. Zeng, Y. He, Y. Liu, R. Liu, Preparation and characterization of reinforced starch-based composites with compatibilizer by simple extrusion, Carbohydr. Polym. 223 (2019) 115122, https://doi.org/10.1016/j.carbpol.2019.115122.
[36] T.J. Gutiérrez, Effects of exposure to pulsed light on molecular aspects of edible films made from cassava and taro starch, Innovative Food Sci. Emerg. Technol. 41 (2017) 387–396, https://doi.org/10.1016/j.ifset.2017.04.014.
[37] O. Lopez, M.A. Garcia, M.A. Villar, A. Gentili, M. Rodriguez, L. Albertengo, Thermo-compression of biodegradable thermoplastic corn starch films containing chitin and chitosan, LWT–Food Sci. Technol. 57 (1) (2014) 106–115.
[38] P. Wongphan, T. Panrong, N. Harnkarnsujarit, Effect of different modified starches on physical, morphological, thermomechanical, barrier and biodegradation properties of cassava starch and polybutylene adipate terephthalate blend film, Food Packag. Shelf Life 32 (2022), https://doi.org/10.1016/j.fpsl.2022.100844.
[39] S.S. de Campos, A. de Oliveira, T.F.M. Moreira, T.B.V. da Silva, M.V. da Silva, J. A. Pinto, A.P. Bilck, O.H. Gonçalves, I.P. Fernandes, M.-F. Barreiro, F. Yamashita, P. Valderrama, M.A. Shirai, F.V. Leimann, TPCS/PBAT blown extruded films added with curcumin as a technological approach for active packaging materials, Food Packag. Shelf Life 22 (2019), https://doi.org/10.1016/j.fpsl.2019.100424.
[40] I. Ilhan, D. Turan, I. Gibson, R. ten Klooster, Understanding the factors affecting the seal integrity in heat sealed flexible food packages: a review, Packag. Technol. Sci. 34 (6) (2021) 321–337.
[41] O.V. López, C.J. Lecot, N.E. Zaritzky, M.A. García, Biodegradable packages development from starch based heat sealable films, J. Food Eng. 105 (2) (2011) 254–263, https://doi.org/10.1016/j.jfoodeng.2011.02.029.
[42] T. Chau, W. Bruckard, P. Koh, A. Nguyen, A review of factors that affect contact angle and implications for flotation practice, Adv. Colloid Interf. Sci. 150 (2) (2009) 106–115.
[43] M. Tavassoli, A. Khezerlou, M.A. Sani, M. Hashemi, S. Firoozy, A. Ehsani, F. Khodaiyan, S. Adibi, S.M.A. Noori, D.J. McClements, Methylcellulose/chitosan nanofiber-based composites doped with lactoferrin-loaded Ag-MOF nanoparticles for the preservation of fresh apple, Int. J. Biol. Macromol. 259 (2024) 129182.
[44] E. Lorencová, P. Vltavská, P. Budinský, M. Koutný, Antibacterial effect of phosphates and polyphosphates with different chain length, J. Environ. Sci. Health A 47 (14) (2012) 2241–2245.